LETTERS

Association of the jets of Enceladus with the warmest regions on its south-polar fractures

Joseph N. Spitale[1] & Carolyn C. Porco[1]

Jets of material have been seen emanating from the south-polar terrain of Saturn's satellite Enceladus[1]. Observations have shown that this region is anomalously warm[2], with the hottest measured temperatures coinciding with the four 'tiger stripe' fractures, named Alexandria, Cairo, Baghdad and Damascus, that straddle the region[1,2]. Here we use Cassini images taken from a variety of viewing directions over two years to triangulate the source locations for the most prominent jets, and compare these with the infrared hotspot locations and the predictions from a recent model of tidally induced shear heating within the fractures[3]. We find that the jets emanate from the four tiger stripes, with the strongest sources on Baghdad and Damascus. All the jets from each fracture seem to lie in the same nearly vertical plane. There is a strong spatial coincidence between our geographical sources and the locations of increased temperature revealed by the infrared experiment. Comparison with the shear heating model shows broad agreement; the exception is the prediction that Baghdad is the least active lineament, whereas we find it to be the most active. We predict that several new hotspots remain to be discovered by future thermal observations.

Positional measurements of 'plumes' (that is, observed features, as opposed to the individual 'jets' of material that can compose a plume, depending on the viewing geometry) were taken from images[4] obtained from a variety of look directions with respect to the surface of Enceladus (Supplementary Table 2) using Narrow Angle Camera on board the Cassini spacecraft. A plume was measured in the two-dimensional image plane by selecting two points: one at the base of the visible plume, and another at higher altitude (Supplementary Figs 1–18). Each of the two points defines a geometrical ray extending from the camera, and the two rays define a plane in space coincident with the plume. The sources of all of the jets contributing to the measured plume must lie somewhere on the ground track formed by the intersection of the plume plane with the surface of the satellite (Fig. 1).

To isolate a particular jet viewed during various imaging sequences from the web of ground tracks derived from all of our images, we looked at the jet directions implied by the intersections of the various plume planes. Assuming that the source locations and the jet directions did not vary significantly throughout the data set, which spans two years, all of the inferred direction vectors as well as the ground-track intersections should be consistent for a given source. Because we found that nearly all of the ground tracks could be associated with some cluster of intersections possessing consistent directions, those assumptions seemed justified. A few of the remaining ground tracks occurred in clusters of two or three and fell in geographically interesting regions—near a tiger stripe or a Cassini Infrared Spectrometer (CIRS) hotspot—so we consider those to be sources as well, but with less confidence. See Supplementary Table 1 for specific details about the identification of each source.

Our solution for the source locations and jet directions consists of eight sources, each on one of the four tiger stripes. We can see a correspondence between our source locations and the hottest CIRS locales: of the six sources that occur in areas covered by the CIRS observations, three overlap CIRS hotspots and a further two are within less than one CIRS footprint of hotspots (Fig. 2). Because the latter two CIRS observations were not accompanied by simultaneous Imaging Science Subsystem imaging, the imperfect correspondence might be explained by errors in 'pointing', that is, locating the CIRS footprint on the surface. The source associated with the largest number of unambiguous sightings (Table 1), source I, was not observed at high resolution by CIRS; however, the CIRS low-resolution brightness temperature map[2] does suggest increased temperatures along the 30° W meridian in that vicinity.

We can also see a correlation between the CIRS temperature of each hotspot[2] and the number of unambiguous sightings of each jet throughout our data set (Fig. 2 and Table 1). This correlation may suggest a direct relationship between temperature and jet strength. If so, we would expect that the CIRS will measure higher temperatures at the location of source I than yet seen elsewhere on the surface, as well as somewhat increased temperatures at sources IV and VII.

The strongest sources (that is, those with the greatest number of sightings throughout our data set) are on Baghdad and Damascus. For each tiger stripe, although individual jets may emerge at oblique angles to the surface, all of the jets on that stripe seem to occupy nearly the same plane, which in all four cases is within a few degrees of being perpendicular to the surface. (Although only one source was identified on Alexandria, it is essentially vertical.) Each of these curtains of jets seems to be well collimated; a measurement of the material seen over the Baghdad stripe in set G suggests that it is confined to about $\pm 10^{\circ}$ of the mean plane, consistent with the scatter observed in the directions of the individual jets (Table 1).

If the largest discrepancies between our source locations and the CIRS hotspot locations—source II versus CIRS F and source V versus CIRS E—result from CIRS pointing errors, then future thermal observations with higher spatial resolution should place those hotspots closer to our source locations. However, tidal-stress calculations[5], which predict that jet activity should be greatest at times when rifts are in tension, show that the area encompassed by CIRS F would have been under compression during most of our observations. Therefore, if that model is correct, it is plausible that the CIRS pointing is accurate and the region instead periodically produces a jet that we were unlucky enough to miss. Indeed, the counts in Table 1 show that jets were more likely to be observed at times when the corresponding regions were predicted to be in tension than in compression. That comparison is clouded by the poor statistics and by the fact that individual jets are often obscured by other jets, depending on the viewing geometry. However, one notable supporting example is provided by the observation that source I, our most obvious source, is

[1]Cassini Imaging Central Laboratory for Operations (CICLOPS), Space Science Institute, 4750 Walnut Street, Boulder, Colorado 80301, USA.

not apparent in set K, despite near-optimum viewing geometry. At the time of that observation, the region around source I was in compression. A more rigorous investigation of the time variability of the jetting and overall plume brightness is planned for a future paper.

Another explanation for the above discrepancies, in addition to the fact that we see no material emanating from CIRS G, might be a change in the jetting activity at those locations during the past millennium in accordance with the 1,000-year cooling timescale arising from thermal simulations[6]; that is, the sub-surface source of the heating may have turned off, but the residual thermal heat has not yet dissipated.

If the planes containing the jets that we have determined for each tiger stripe reflect the orientations of the corresponding fissures, then those fissures are essentially vertical. That orientation may be consistent with their formation as tensile cracks under the current stress regime, because the current orientation of the tiger stripes corresponds to nearly maximum normal tidal stress[3]. Alternatively, jetting has been observed elsewhere in the Solar System with no apparent confining vent[7], so the collimation may instead arise from other physical processes. However, this non-confined jetting was vertical and, although our plume planes are vertical, not all of the individual jets contained in those planes emerge vertically.

Localized heating resulting from tidally driven strike–slip motion along the tiger stripes has been proposed as a source of the anomalous heat radiating from the tiger stripes, which in turn powers the jets[3]. That calculation predicts maximum heating on Alexandria around 150° W longitude (very close to source IV), on Cairo around 60° W longitude close to source V (CIRS E) as well as at 120° W near source VIII (CIRS B), on Damascus near sources II and III, and on the lower latitude branch of Damascus near CIRS F. Minimal heating is predicted on Baghdad, although a small region near source VI (CIRS C) does show a significant signal. There are a few additional small regions where that model predicts increased heating and where we see no jets. Thus, although that calculation successfully predicts most of our observed jets, it fails to explain the fact that we observe Baghdad to be the most active tiger stripe on the basis of the sighting counts in Table 1 and supported by increased CIRS brightness temperatures in that vicinity. It does corroborate the location of CIRS F, lending additional support to the idea that it is the site of a jet that was in the dormant part of its cycle at the times of our observations, instead of a mis-registered CIRS footprint. It also corroborates source II. Therefore, if the pointing for CIRS F is accurate, then the

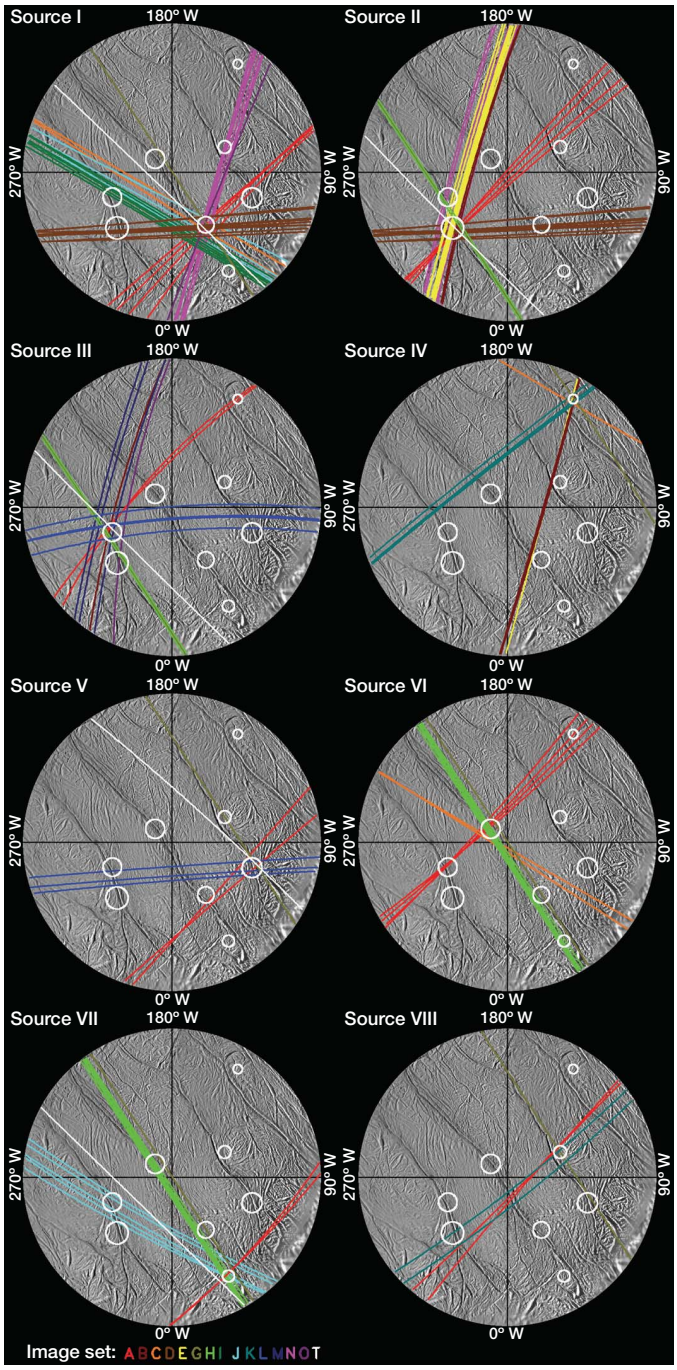

Figure 1 | Stereographic projections with ground tracks for each source solution. Each image set is denoted by a unique colour. Circles encompass the standard deviation of the cluster of intersections comprising each source. Some ground tracks are shown for more than one source because the unique source cannot be distinguished (for example, sets G and H, viewing along the tiger stripes). Source numbers are shown on the larger map in Fig. 2. Where necessary to bring out detail, image sets were averaged before measuring, and hence show only one ground track (see Supplementary Figs 1–18).

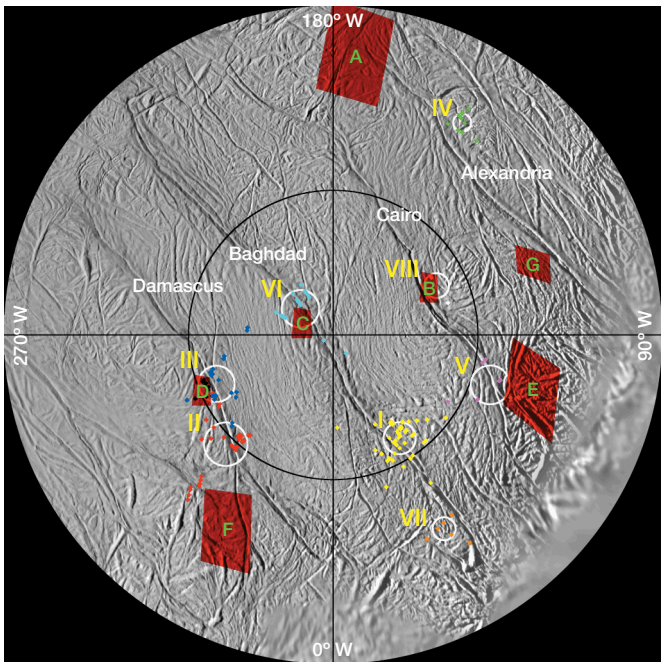

Figure 2 | Stereographic projection of the south-polar terrain showing our sources and CIRS hotspots. Our source locations are labelled with yellow roman numerals; CIRS hotspots are labelled with green capital letters. The intersections comprising each source are shown as coloured diamonds. Circles represent the standard deviations of those sets of intersections. Intersections of planes separated by less than 20° were excluded because the precise location of those intersections is overly sensitive to small variations in the plane orientations.

Table 1 | Jet source locations, directions, sighting counts and CIRS hotspot associations

Source	Tiger stripe	Lat. (°)	Lon. (° W)	σ (°)	Azimuth (°)	Zenith (°)	σ (°)	#T	#C	#CT	#TC	Sightings	CIRS (ref. 2)	Temperature (K) (ref. 2)
I	Baghdad	−81.5	32.8	1.6	(228.7)	9.7	9	3/5	1/2	2/3	1/1	7	–	–
II	Damascus	−79.4	315.5	2.1	(93.8)	6.8	9	3/5	0/0	0/0	0/0	5	(F)	157 ± 24
III	Damascus	−81.3	292.8	1.8	83.2	30.2	10	3/6	0/2	2/2	0/0	6	D	145 ± 14
IV	Alexandria	−72.9	148.7	0.7	(110.0)	3.7	15	0/0	1/3	1/1	0/0	4	–	114 ± 22
V	Cairo	−78.6	72.3	1.7	(229.8)	6.0	5	0/3	3/6	0/0	0/0	3	E	133 ± 28
VI	Baghdad	−87.1	231.4	1.8	(187.6)	10.2	2	1/4	1/2	0/0	0/0	2	C	135 ± 9
VII	Baghdad	−74.6	29.8	1.1	352.5	20.8	5	2/6	0/3	0/0	0/0	3	–	–
VIII	Cairo	−82.1	115.5	1.0	(127.7)	6.8	12	1/3	0/4	0/2	0/0	2	B	117 ± 16
													G	127 ± 28

Latitudes (Lat.) are planetographic and longitudes (Lon.) increase toward the west. Azimuths are measured clockwise from local north (that is, eastward to an observer standing on the surface facing north); values in parentheses are poorly determined owing to the small zenith angle (angle measured from the vertical). The uncertainties σ corresponds to the standard deviation in the spherical coordinates corresponding to the set of vectors comprising each quantity (source location or jet direction). Columns labelled with # record the number of times a source was unambiguously detected in a given stress state[5]—T, tension; C, compression; CT, transitioning from compression to tension; and TC, transitioning from tension to compression—compared with the number of times it might have been seen in that state in our data set. This count excluded sightings from sets G and H because that geometry (looking along the tiger stripes) did not allow us to determine which particular jets were active on a given tiger stripe at those times. The set D observations were also excluded because they cannot be linked uniquely to either source I or II. We counted sightings in multiple images within a single image set only once. Configurations for which it was difficult to determine the prevailing stress state at that location at that time were not counted. Totals for all sources are given in the bottom row. CIRS hotspot associations in parentheses are questionable. '–' indicates that there is no associated hotspot.

region containing source II was never observed by CIRS and we would expect an additional hotspot to be found there.

Received 17 May; accepted 30 August 2007.

1. Porco, C. C. *et al.* Cassini observes the active south pole of Enceladus. *Science* **311,** 1393–1401 (2006).
2. Spencer, J. R. *et al.* Cassini encounters Enceladus: background and the discovery of a south polar hot spot. *Science* **311,** 1401–1405 (2006).
3. Nimmo, F. *et al.* Shear heating as the origin of the plumes and heat flux on Enceladus. *Nature* **447,** 289–291 (2007).
4. Porco, C. C. *et al.* Cassini imaging science: instrument characteristics and anticipated scientific investigations at Saturn. *Space Sci. Rev.* **115,** 363–497 (2004).
5. Hurford, T. A. *et al.* Eruptions arising from tidally controlled periodic openings of rifts on Enceladus. *Nature* **447,** 292–294 (2007).
6. Spencer, J. R. *et al.* The south polar hot spot on Enceladus. *Lunar Planet. Sci. Conf.* **XXXVII,** 2252 (2006).
7. Milazzo, M. P. *et al.* Observations and initial modeling of Lava-SO2 interactions at Prometheus, Io. *J. Geophys. Res.* **106 E12,** 33121–33128 (2001).

Supplementary Information is linked to the online version of the paper at www.nature.com/nature.

Acknowledgements We thank Paul and Pauline Helfenstein for the planning of the Enceladus plume observations and the staff members at the CICLOPS for technical support. D. Wilson at CICLOPS provided assistance with image processing. We thank H. J. Melosh, A. P. Ingersoll and P. Helfenstein for their comments. This work was funded by the Cassini project.

Author Contributions Both authors devised the approach and contributed equally to the discussion and conclusions. J.N.S. executed the work, produced the solutions and wrote most of the text. C.C.P. instigated the work and revised the text.

Author Information Reprints and permissions information is available at www.nature.com/reprints. Correspondence and requests for materials should be addressed to J.N.S. (spitale@lpl.arizona.edu).

SUPPLEMENTARY INFORMATION

1. Description of source identifications

Strongest Candidate Sources -- I, II, III, and VI

Our initial survey revealed three strong candidate sources, followed later by a fourth, all lying on the Baghdad and Damascus lineaments. We labeled these sources I, II, III, and VI. These sources account for a significant number of intersecting ground tracks and remove the need to postulate sources in that region that do not lie near tiger stripes. Source III correlates well with CIRS hot spot D and is notable for its rather non-vertical zenith angle. Source II lies about 13 km from CIRS hot spot F, a distance that amounts to less than one pixel for that particular CIRS observation. Source I lies in a region not yet sampled by the CIRS experiment. Source VI, the brightest plume in set A, lies very close to the south pole and correlates well with CIRS hot spot C, their hottest measurement.

Source IV

Observation G-3 implies at least one source along the Alexandria lineament. Three other observations -- B-4, C-3, and K-2 -- cross G-3 at about the same point on the surface. Moreover, although observations B-4 and K-2 each cross two other identified sources (B-4 passes near sources I and VIII; K-2 passes near sources III and VI), their directions are consistent only near where they cross Alexandria. C-3 crosses no other tiger stripes. Therefore, we suggest source IV as the most likely location for an Alexandria source. One problem with this identification is that the direction vectors formed by the plane intersections at source IV are not as tightly clustered as we would prefer for a confident identification. However, the standard deviation is skewed by a single outlying direction vector that is fairly uncertain because it corresponds to the intersection of two plume planes -- C-3 and G-3 -- that, while not quite parallel enough to summarily reject, yield a

suspicious direction vector. This source does not clearly correspond to any identified CIRS hot spot, but it does occur in a region of fairly low-resolution CIRS coverage in which a hot spot has been identified.

Source V

Source V lies at the intersection of observations L-1 and A3-4 with G-4, on the Cairo tiger stripe. Both ground tracks L-1 and A3-4 cross other sources, but the computed directions at those intersections are not consistent with those other sources. The L-1 and A3-4 observations cross other tiger stripes and might suggest other sources than those we have identified, but only at source V do those observations comprise a multiple intersection with consistent direction vectors. CIRS hot spot E lies quite close to source V, so we suspect an association.

Source VII

Source VII lies near the western end of the Baghdad tiger stripe. Observations A1-6, A2-7, A3-6, and A4-7 (the same jet seen from four slightly different angles in the November 2005 movie) skirt the ends of the tiger stripes and might be argued to correspond to sources on Alexandria, or on Cairo near CIRS E, rather than on Baghdad. However, the J-2 observation, which crosses Damascus near sources II and III is consistent with neither of those sources, and therefore likely corresponds to a source on Baghdad. T-5 does not approach any other known sources and all of the above observations taken together give a consistent direction vector.

Source VIII

After accounting for sources I through VII and ignoring the numerous smaller plumes in

the higher-resolution image sets (A, B, and T), and the problematic high-phase observations of set O (see below), we are left with a single observation: K-1. The K-1 ground track crosses all four tiger stripes. It passes near source II on the Damascus stripe, but its direction is not consistent with that source. There are no other imaging observations that allow us to confidently narrow the source location to one of the three remaining stripes. However, because the intersection of the K-1 ground track with the Cairo tiger stripe correlates well with the location of CIRS hot spot B, we favor Cairo as the location of the K-1 source. Observations A2-6 and A3-10 give consistent direction vectors at this location as well, but the same can be said of the location where those two tracks and K-1 intersect Baghdad.

Source	Observations
I	A1-3, A2-5, A3-3, A4-4, C-2, G-1, I-1, J-1, N-2, O-1
II	A1-2, A2-2, A3-2, A4-2, B-1, D-1, E-1, G-2, H-2, N-1
III	A2-10, A3-9, B-2, G-2, H-2, L-2, M-1, O-2, T-10
IV	B-4, C-3, E-2, G-3, K-2
V	A3-4, A4-5, G-4, L-1, T-2
VI	A1-1, A2-1, A3-1, A4-1, C-1, G-1, H-1
VII	A2-7, A3-6, G-1, H-1, J-2, T-5
VIII	A2-6, A3-10, G-4, K-1

Supplementary Table 1. Table of plume observations identified for each source. See Supplementary Figs. 1 -- 18 for observation labels.

2. Data Table

Set	Date	Images	Scale (km/pixel)	Phase (deg)	S/C Lat. (deg)	S/C W. Lon (deg)
A1 A2* A3* A4	2005-331	N1511804720 N1511805412 N1511805445 N1511805493 N1511806152 N1511806200 N1511803932	0.864	161.	0.9	131.
B	2005-331	N1511812952 N1511812985	1.05	161.	0.9	164.
C	2005-048	N1487334245 N1487335135	1.84	153.	0.6	238.
D	2006-018	N1516298124 N1516298143 N1516298169 N1516298348 N1516298367 N1516298566 N1516298600 N1516299025 N1516299163	5.99	150.	0.3	92.2
E	2006-018	N1516320030 N1516320064 N1516320083 N1516320102 N1516320128 N1516320323 N1516320591	5.57	154.	0.4	164.
G*	2006-081	N1521714316 N1521714411 N1521714498 N1521714566 N1521715294	7.81	160.	0.3	32.6
H	2006-082	N1521837867 N1521837925 N1521837962 N1521837988 N1521838030	11.5	161.	0.3	33.0
I	2006-083	N1521903967 N1521904025	11.1	162.	0.4	239.

		N1521904062 N1521904088 N1521904175 N1521904209 N1521904243				
J	2006-123	N1525337880 N1525337906 N1525337948 N1525337982 N1525338585	11.7	163.	0.3	240.
K	2006-123	N1525360823 N1525360860 N1525360928 N1525360996 N1525361030	13.7	163.	0.3	308.
L	2006-124	N1525413188 N1525413225 N1525413251 N1525413395	13.5	157.	0.3	93.8
M	2006-124	N1525435485 N1525435511 N1525435553	12.6	159.	0.3	165.
N	2006-223	N1533960372 N1533960491 N1533960525 N1533960567 N1533960609 N1533960651 N1533960693 N1533961239	12.9	164.	7.	163.
O*	2006-258	N1537033403 N1537033496	11.7	178.	17	158.
T*	2007-114	N1556118855 N1556118944 N1556118977 N1556119025 N1556119080 N1556119135 N1556119279 N1556119437 N1556119477	1.08	159.	-8.	226.

Supplementary Table 2. Table of images used in this study. The observations were distributed in phase angle from 148° to 178°. The lowest resolution image used in this study has a spatial scale of about 14 km/pixel. Because of the tenuous nature of the jets and the (inferred) predominance of micron-sized particles, jets have been seen only in images obtained at high phase geometries – i.e., phase angles greater than about 150° – where tiny particles are bright due to diffraction scattering of light (the ISS does not sense vapor in these images). For most images, the sub-spacecraft latitude was within a few degrees of Enceladus' equator, putting the south pole close to the satellite's limb. In one image, the sub-spacecraft latitude was ~ 15° N. In most cases, the named images were measured individually. In a few cases (indicated by an asterisk next to the set label), the images were summed.

3. Figures showing plume measurements and labels.

The following figures show all of the measured plumes. Many of the measurements were trivial to carry out, but some of the lower resolution images posed a challenge and are difficult to display here convincingly. We used only images with lossless or no compression and we did not use measurements that we could not reproduce by remeasuring the same plumes at a later date.

Unlike the other image sets, set A consists of four separate geometries, each separated by about 10 minutes, during which the viewing angle changed enough that individual plumes were not always clearly identifiable throughout the sequence. Therefore, set A was decomposed into four subsets -- A1, A2, A3, and A4 -- in which the plumes were measured and labeled independently.

All images were calibrated. Sets A2, A3, G, O, and T were also sky subtracted (the "sky" was computed by averaging along horizontal and vertical lines in blank regions of the image) and the images indicated in Supplementary Table 2 were averaged together. All images were stretched to enhance contrast.

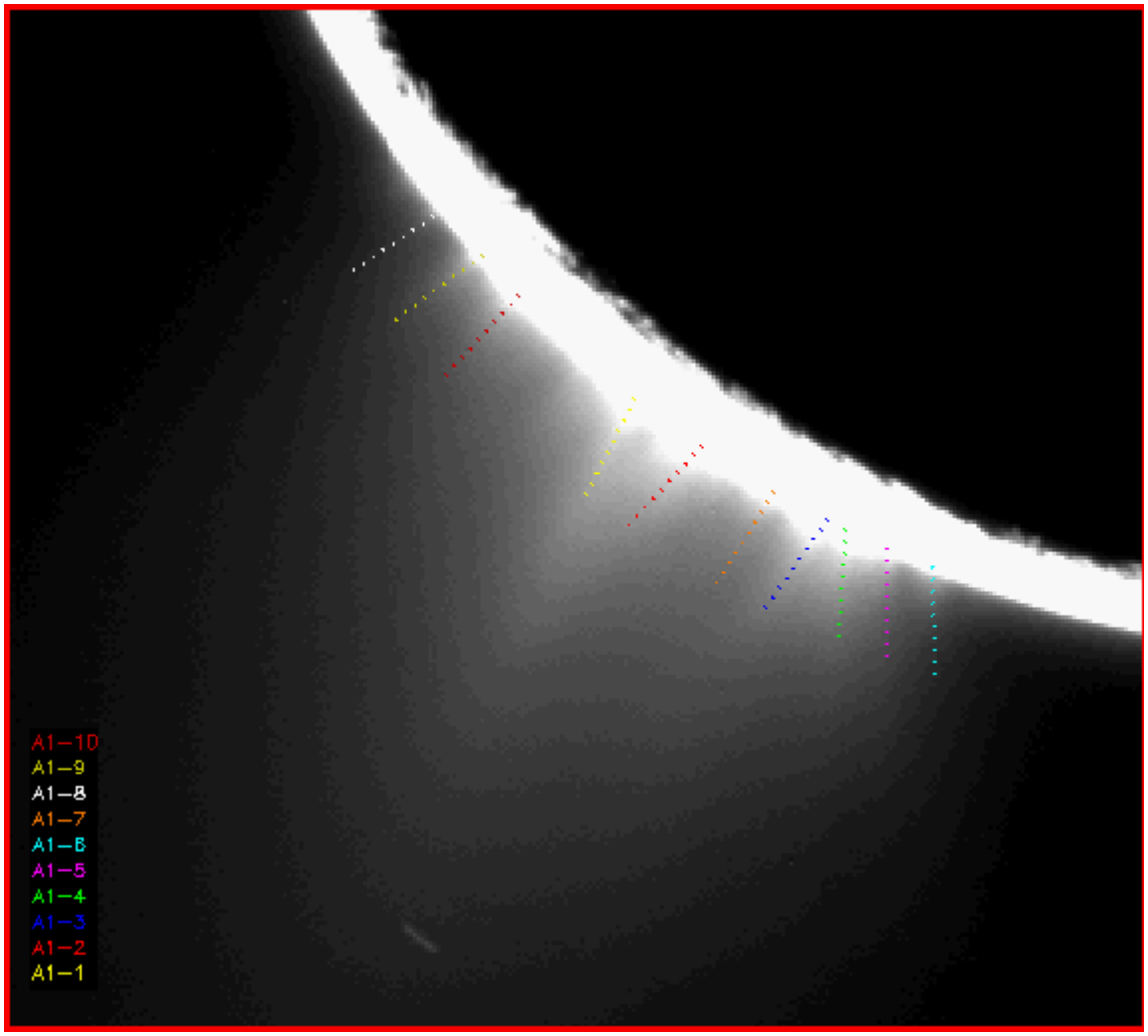

Supplementary Figure 1. Set A1 measured plumes. This image was calibrated and stretched.

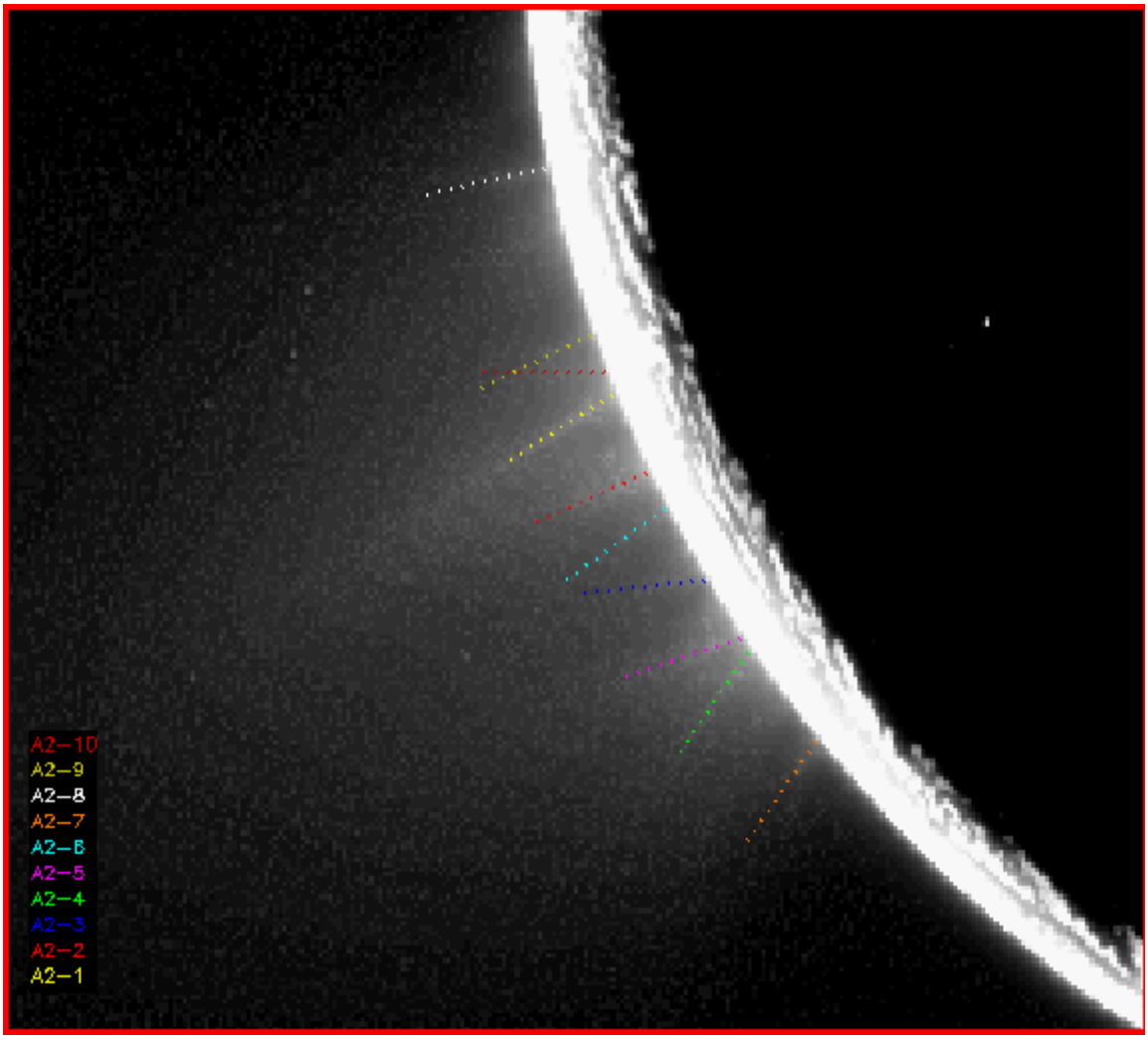

Supplementary Figure 2. Set A2 measured plumes. Three calibrated images were co-added and a sky subtraction was performed. The final image was stretched.

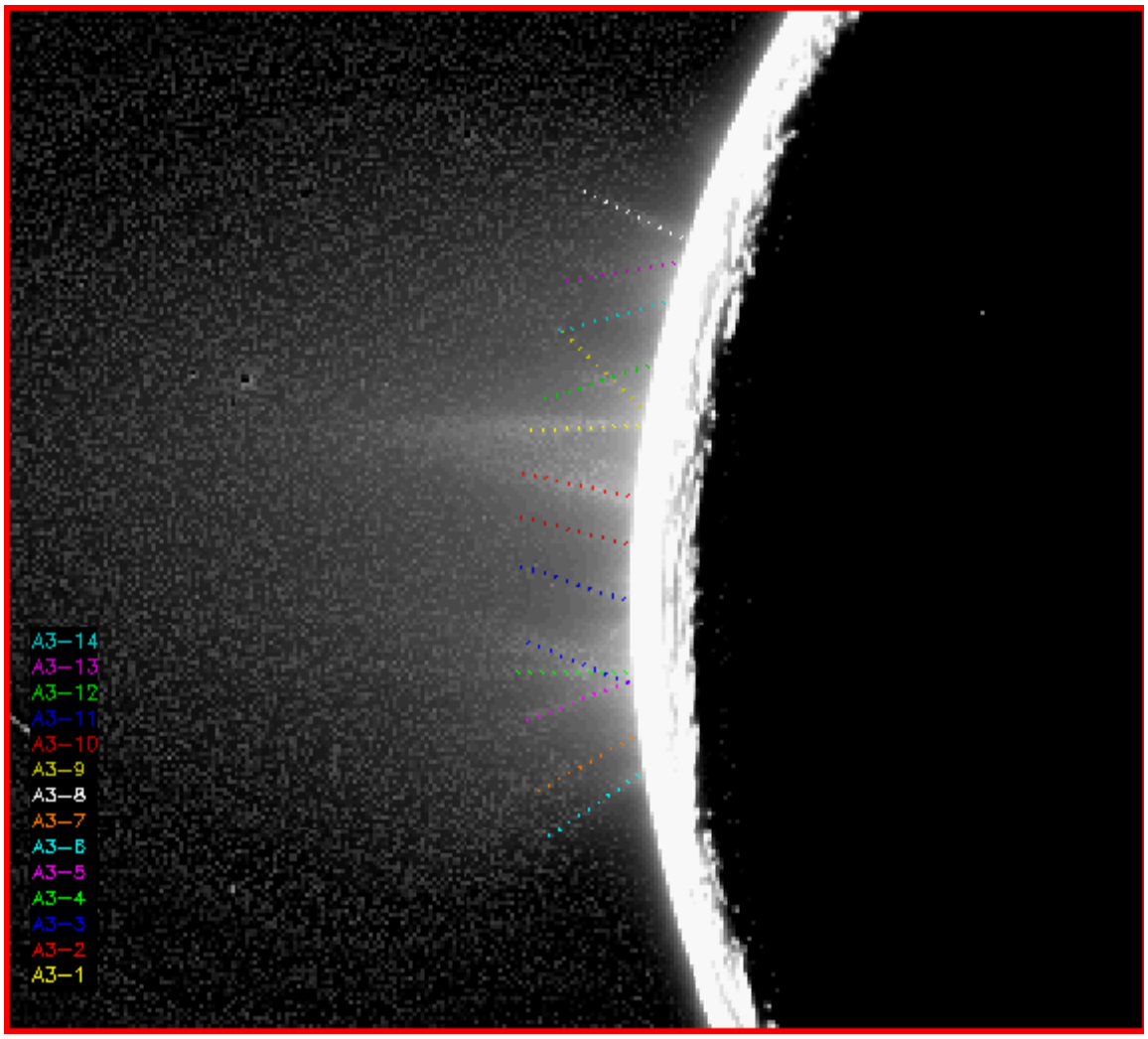

Supplementary Figure 3. Set A3 measured plumes. Two calibrated images were co-added and a sky subtraction was performed. The final image was stretched.

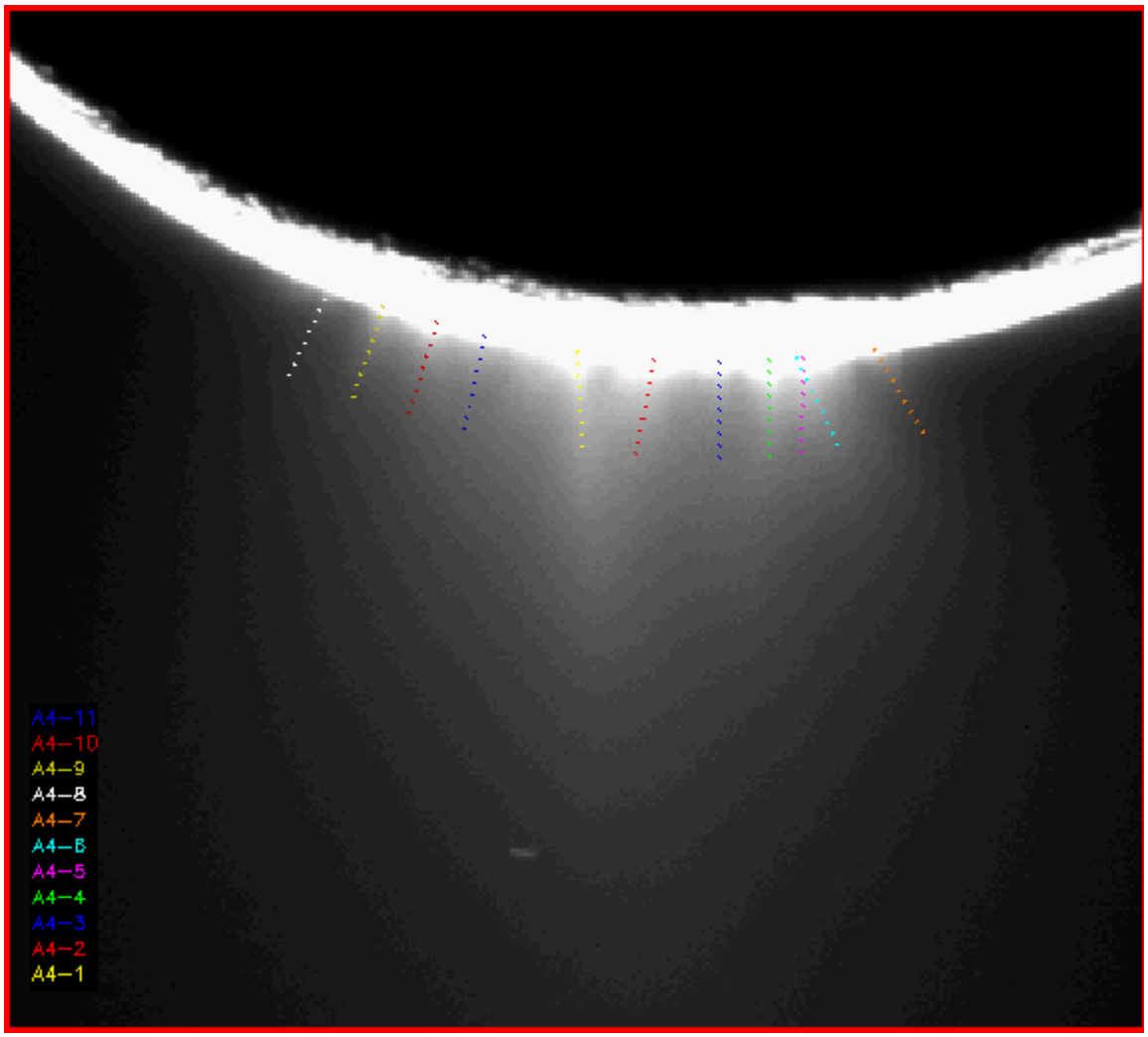

Supplementary Figure 4. Set A4 measured plumes. This image was calibrated and stretched.

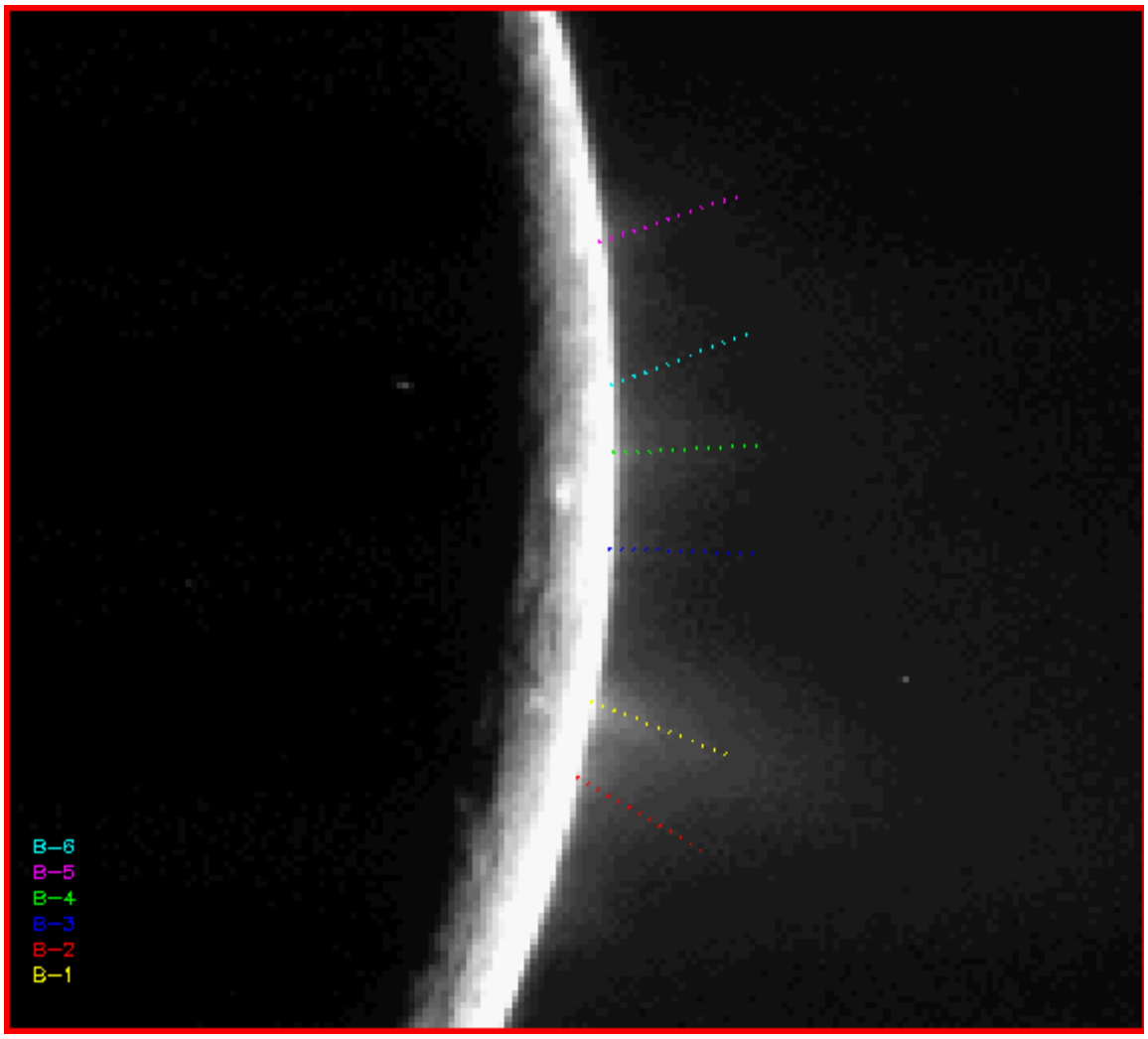

Supplementary Figure 5. Set B measured plumes. This image was calibrated and stretched.

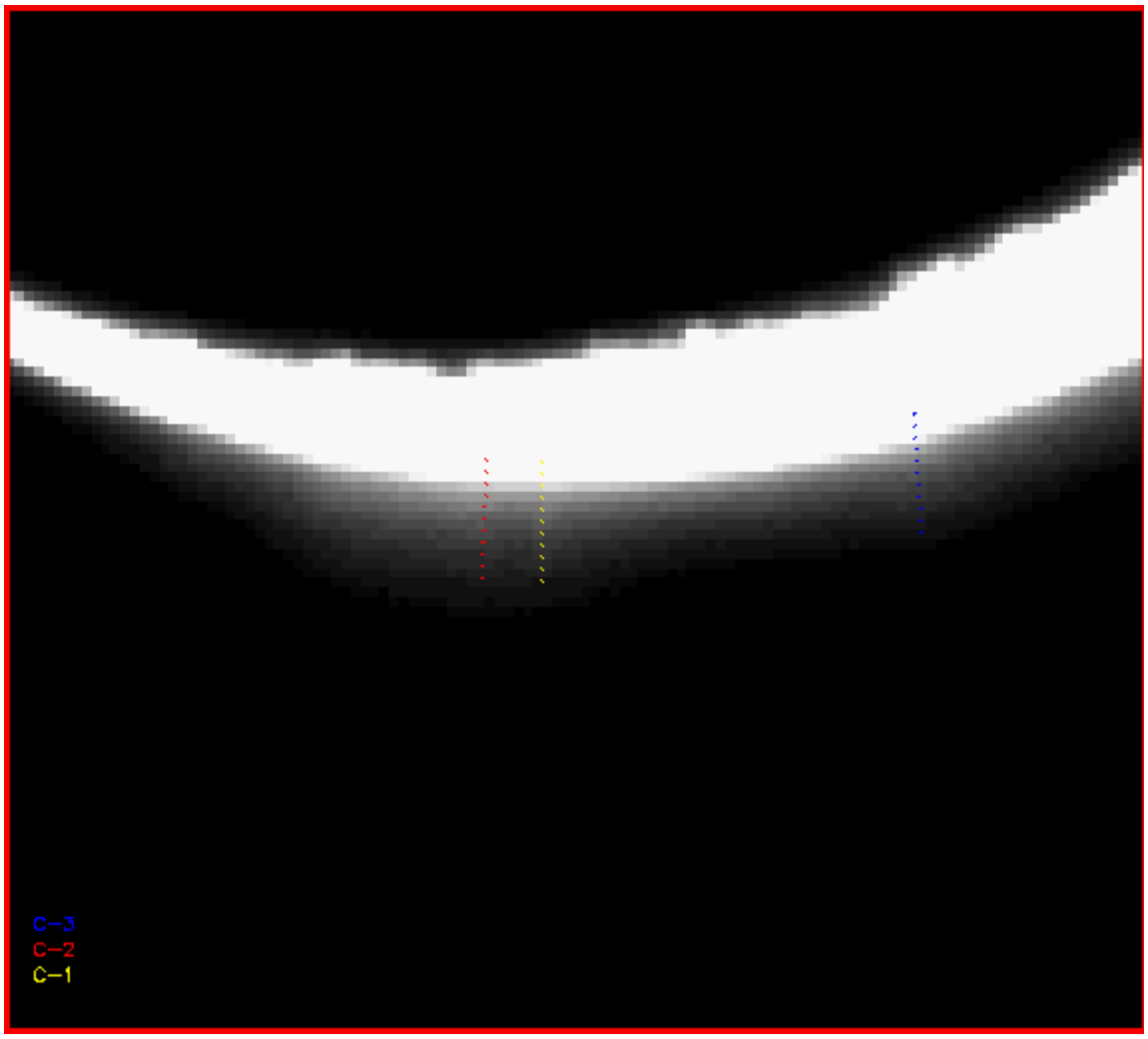

Supplementary Figure 6. Set C measured plumes. This image was calibrated and stretched.

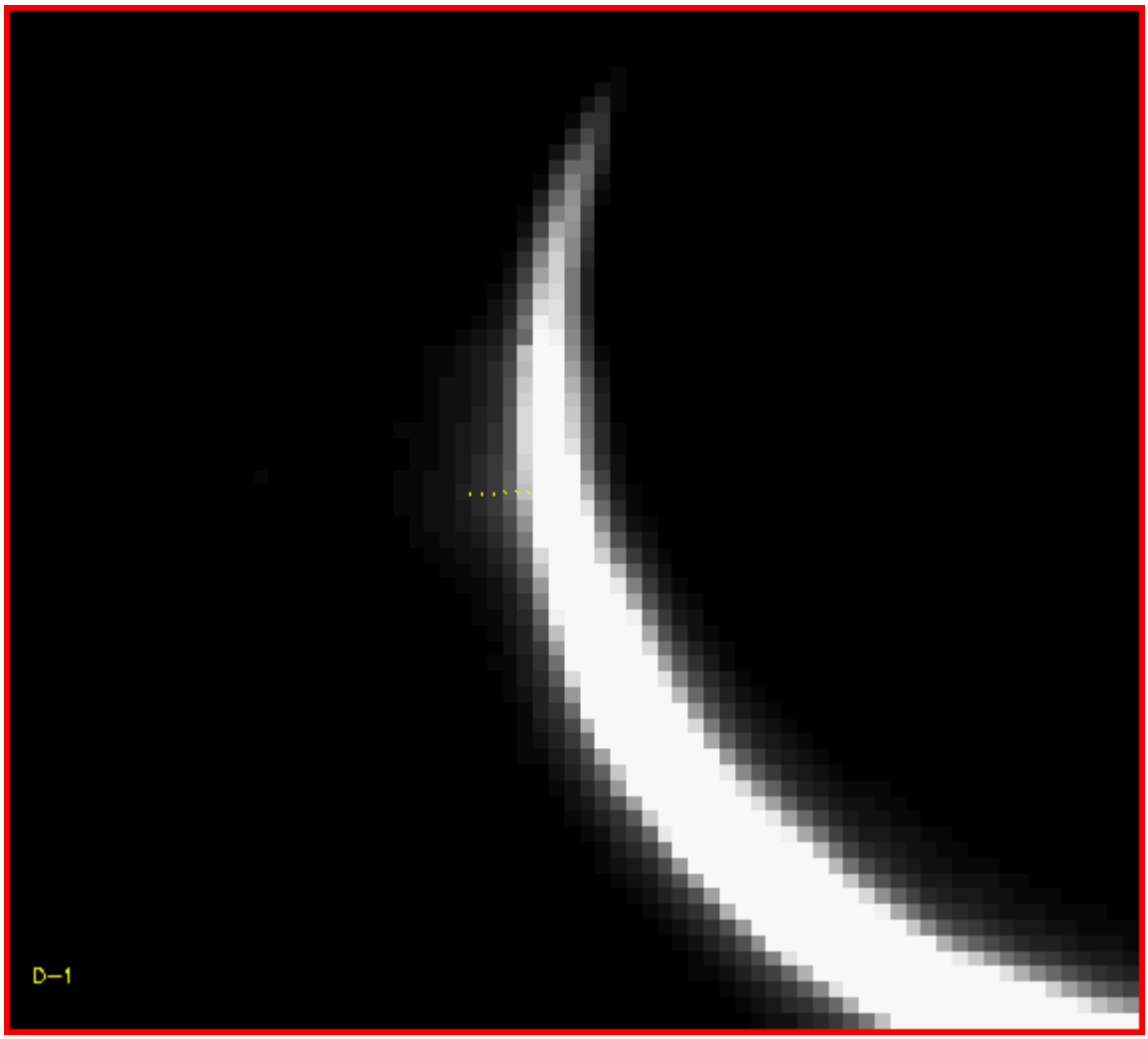

Supplementary Figure 7. Set D measured plumes. This image was calibrated and stretched.

Supplementary Figure 8. Set E measured plumes. This image was calibrated and stretched.

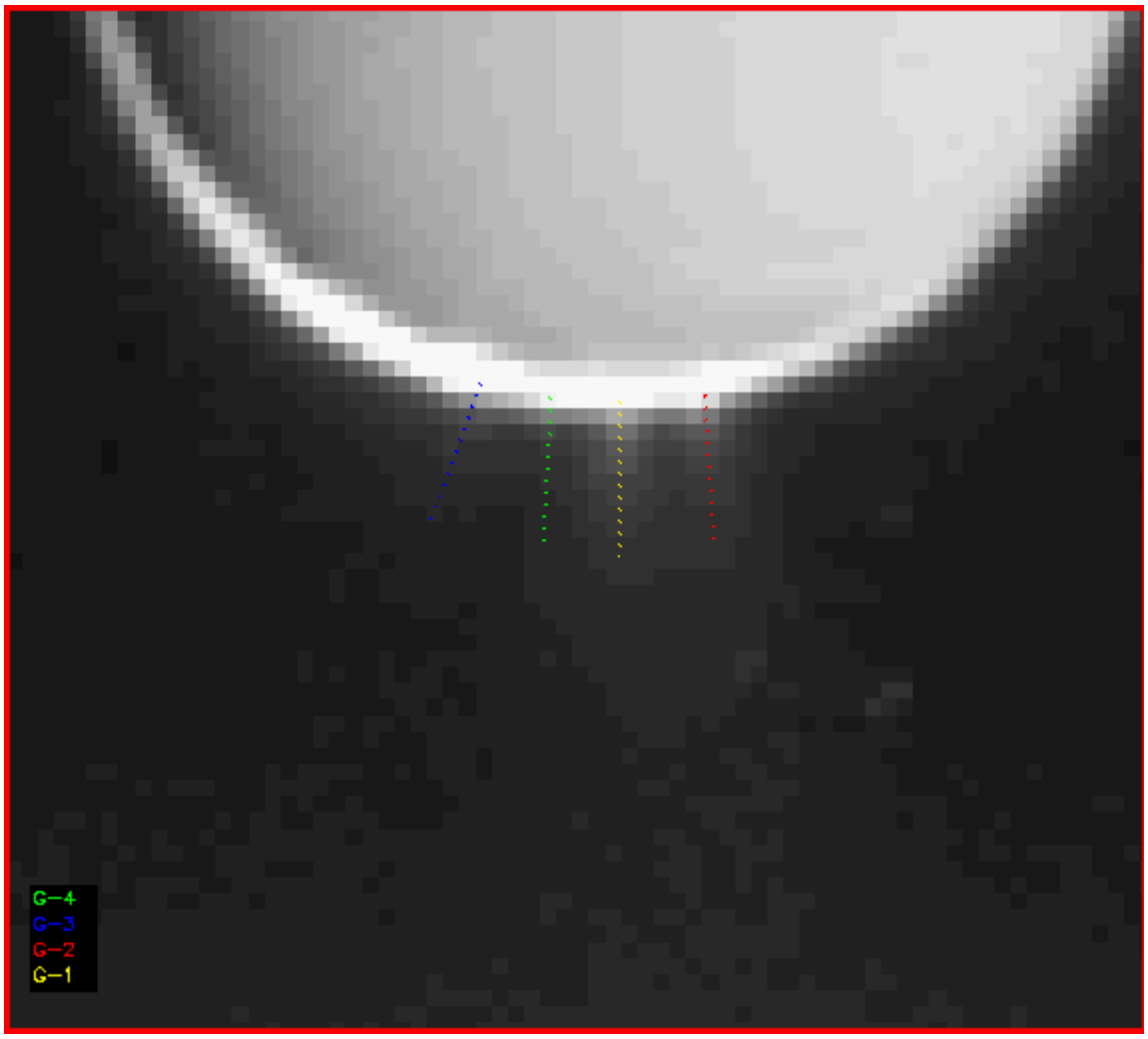

Supplementary Figure 9. Set G measured plumes. Five calibrated images were co-added and a sky subtraction was performed. The final image was stretched.

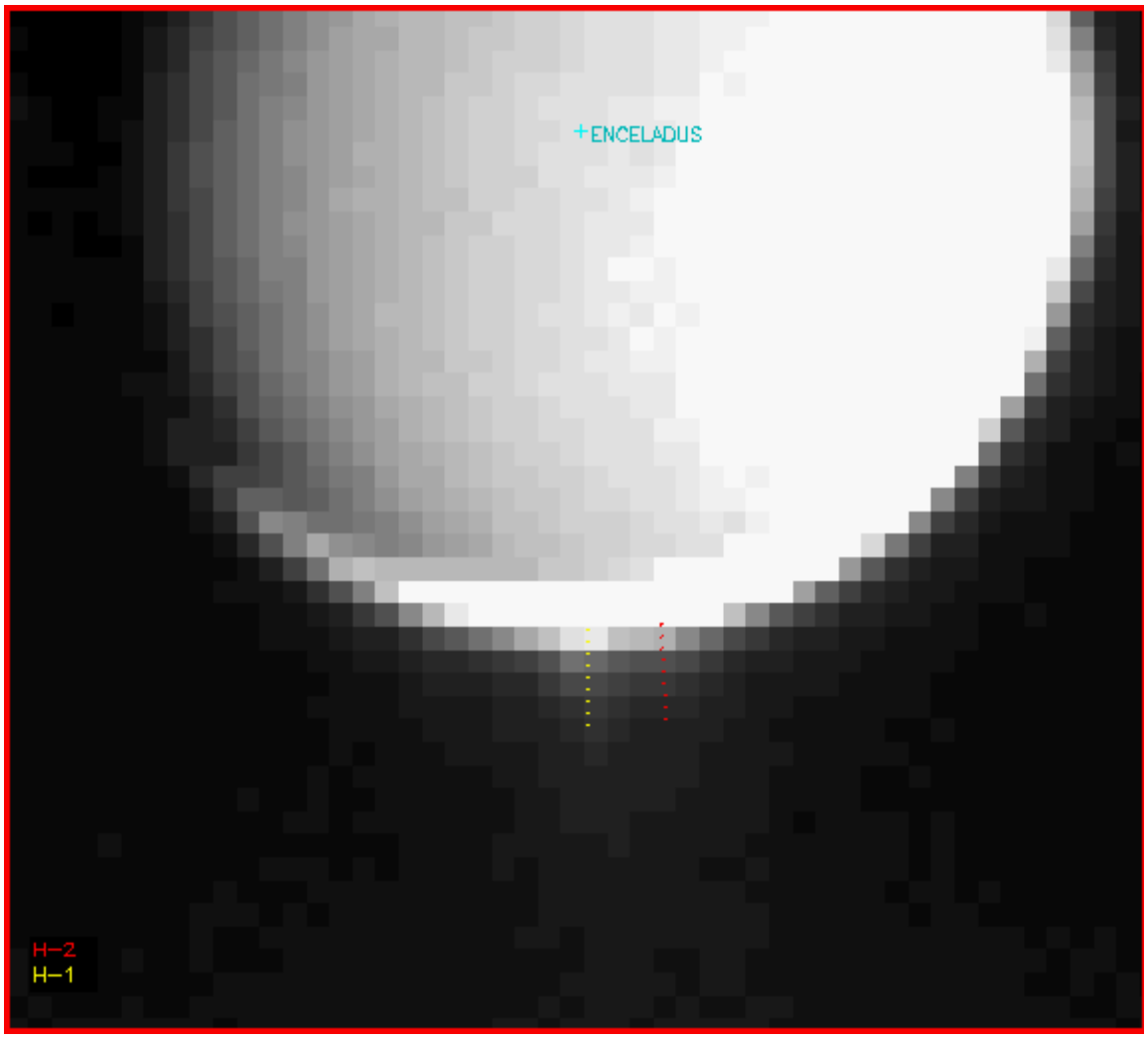

Supplementary Figure 10. Set H measured plumes. This image was calibrated and stretched.

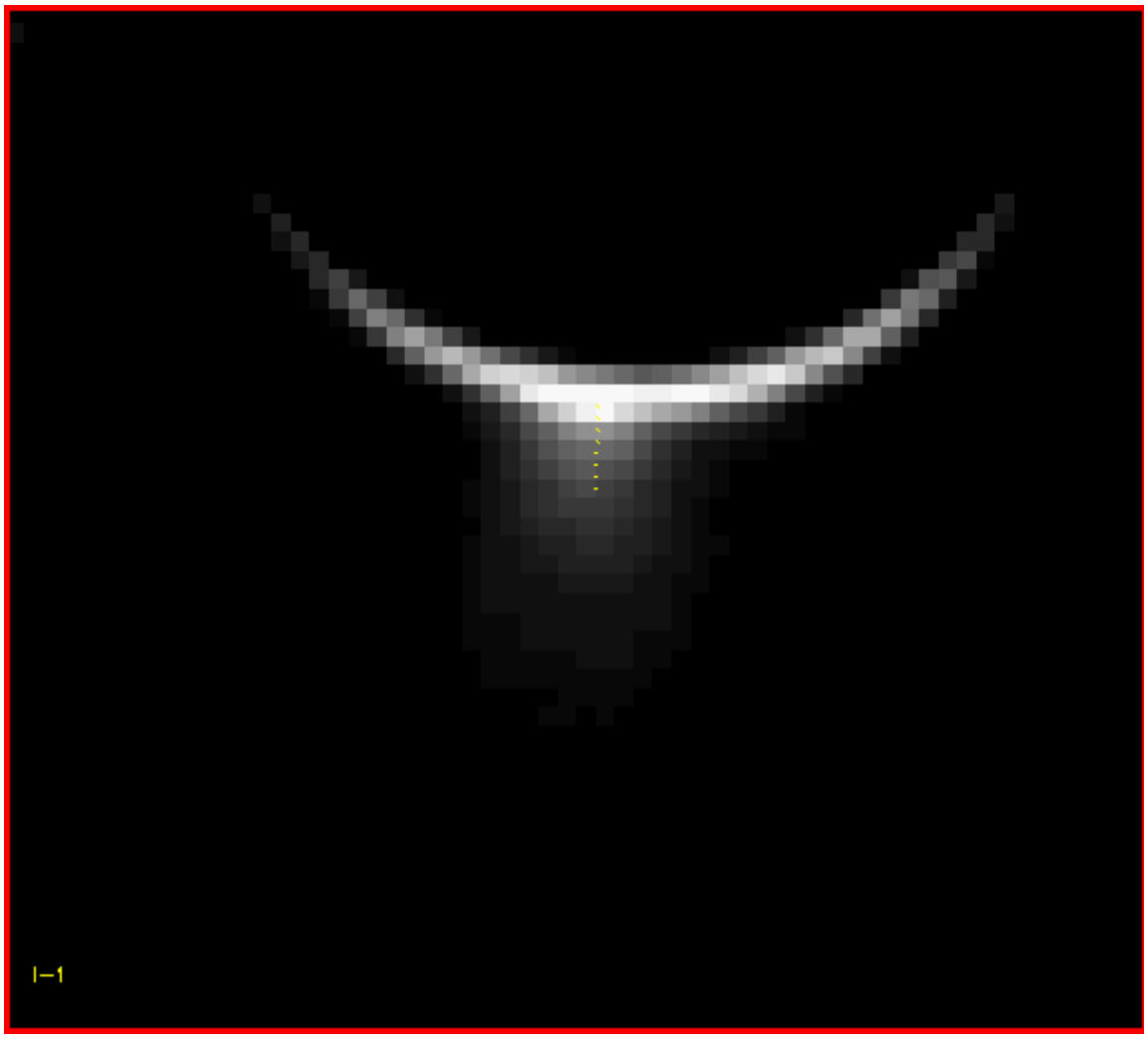

Supplementary Figure 11. Set I measured plume. This image was calibrated and stretched.

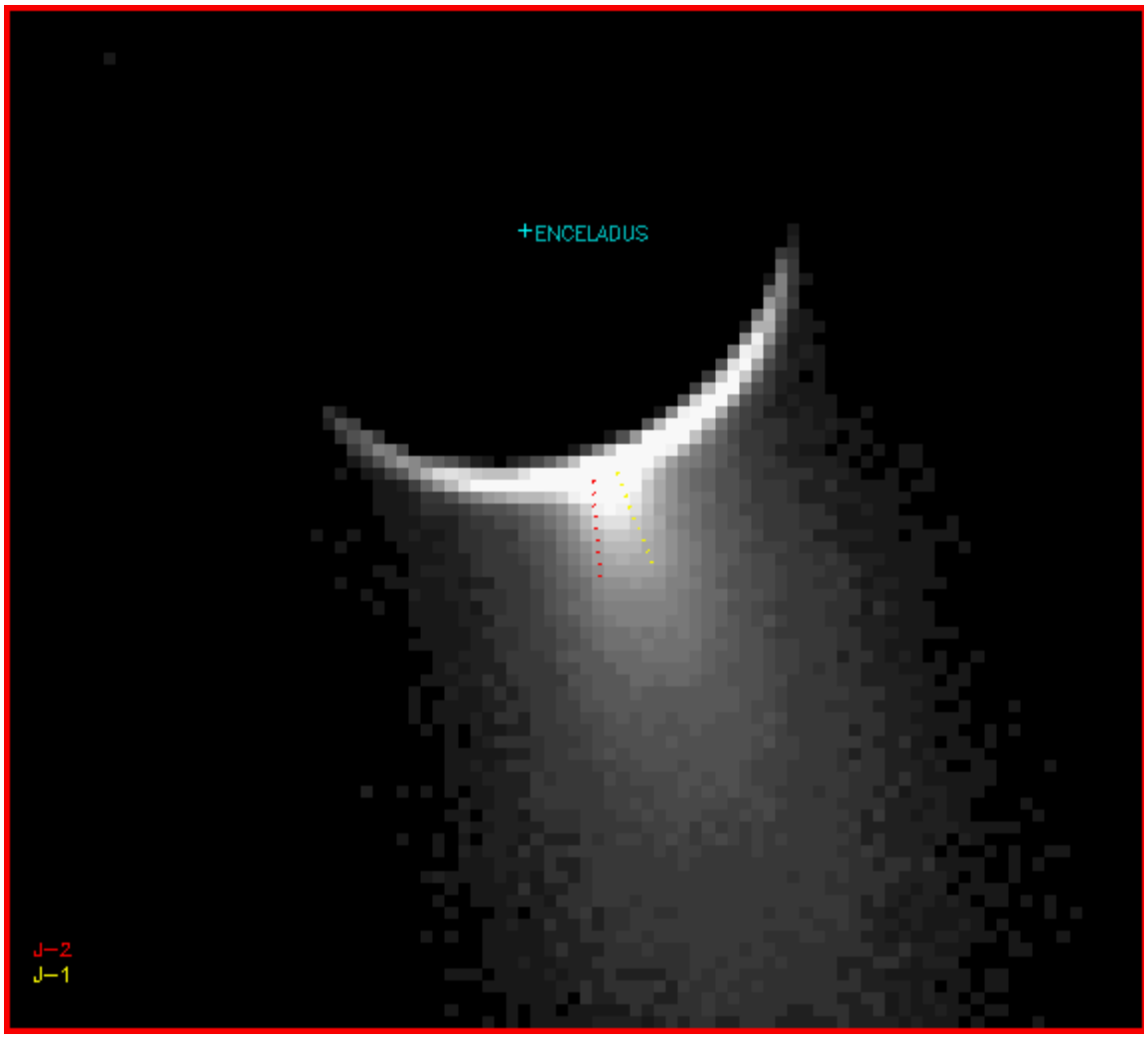

Supplementary Figure 12. Set J measured plumes. This image was calibrated and stretched.

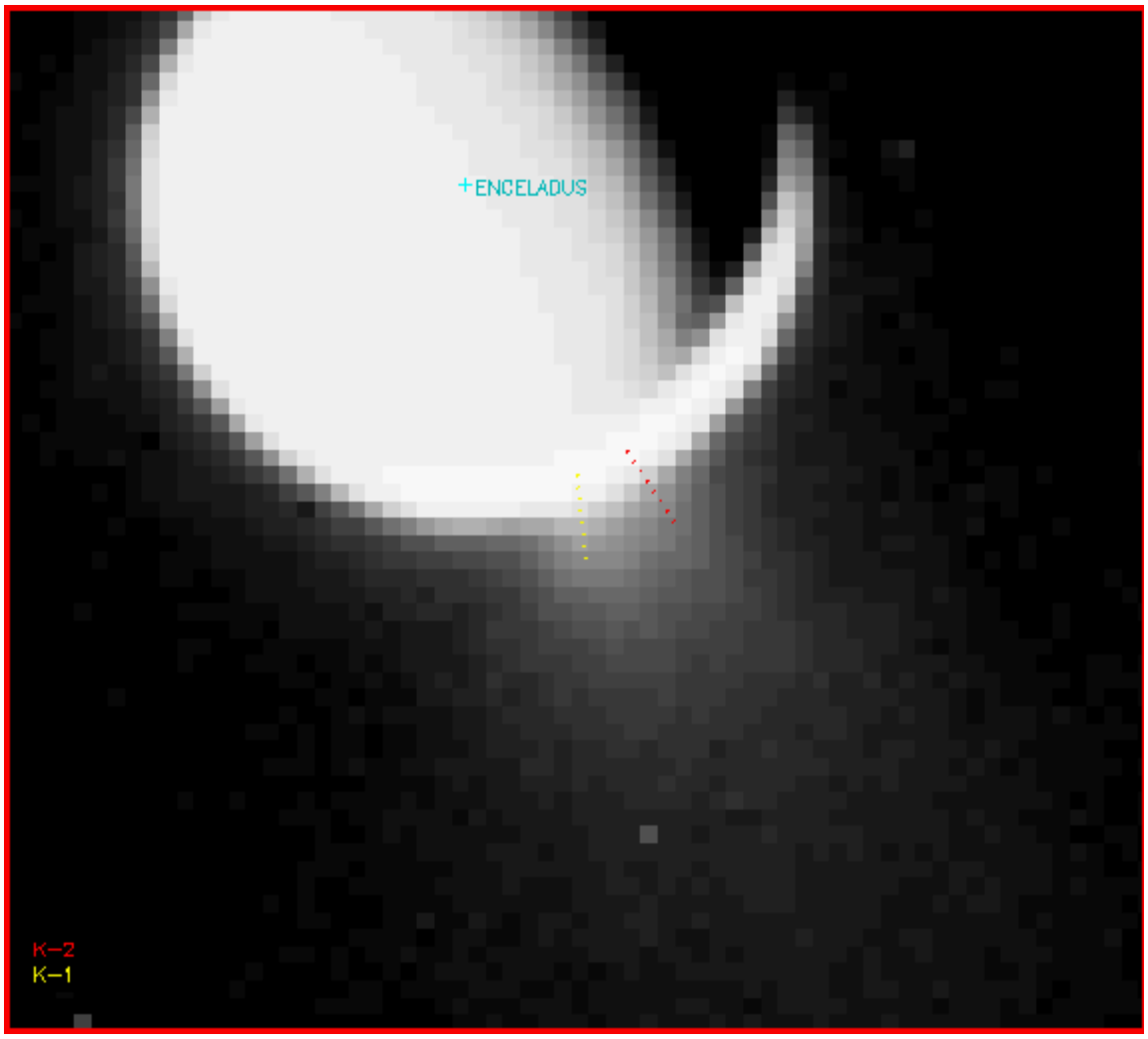

Supplementary Figure 13. Set K measured plumes. This image was calibrated and stretched.

Supplementary Figure 14. Set L measured plumes. This image was calibrated and stretched.

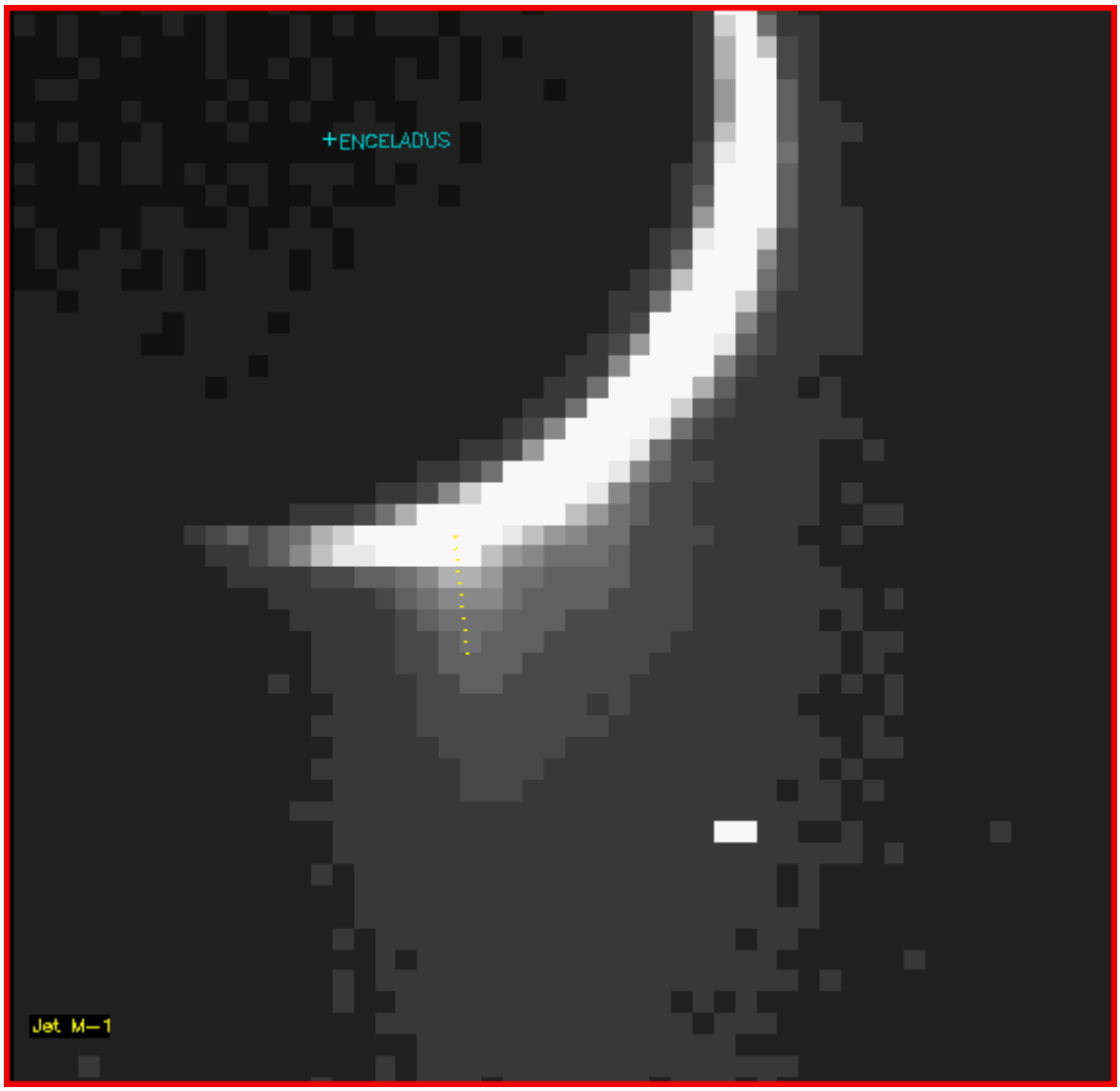

Supplementary Figure 15. Set M measured plume. This image was calibrated and stretched.

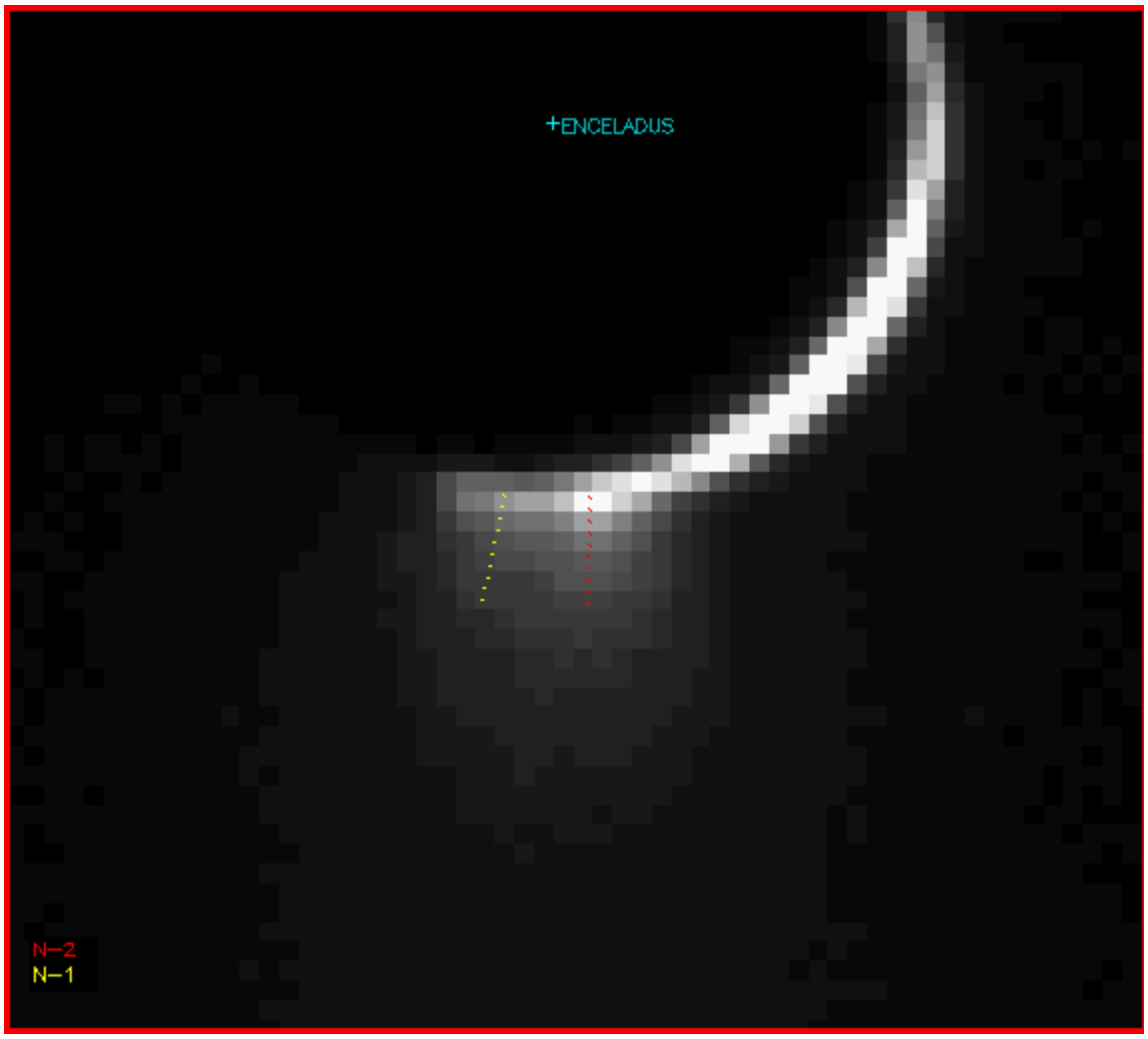

Supplementary Figure 16. Set N measured plumes. This image was calibrated and stretched.

Supplementary Figure 17. Set O measured plumes. Two calibrated images were co-added and a sky subtraction was performed. The final image was stretched. This set of observations was obtained at thehighest phase angle in our study. The enhancement reveals considerable structure, but only the two most prominent features correlate with with our identified sources. Some uncertainty arises from the fact that these observations were obtained at a significantly more northern sub-spacecraft latitude than the others (meaning that the sources are further behind the limb); however, we suspect that much of the detail corresponds to structures in the field of view upstream or downstream in Enceladus' orbit, not directly connected to the satellite.

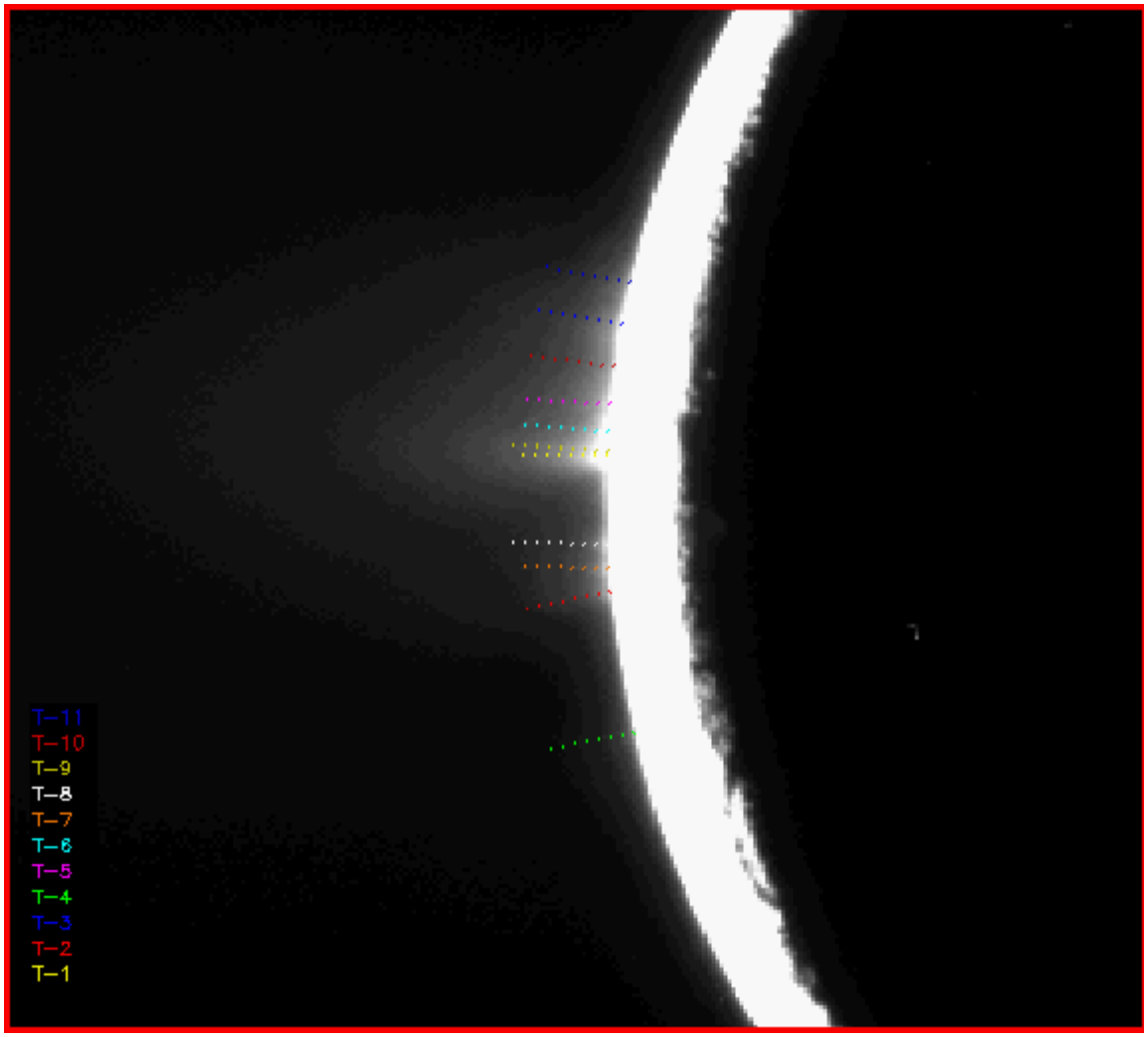

Supplementary Figure 18. Set T measured plumes. Nine calibrated images were co-added and a sky subtraction was performed. The final image was stretched.